

# Quantum Fluctuations in a Weakly Correlated Mott Insulator

Qisi Wang,<sup>1, 2, \*</sup> S. Mustafi,<sup>2</sup> E. Fogh,<sup>3</sup> N. Astrakhantsev,<sup>2</sup> Z. He,<sup>4, 5</sup> I. Bialo,<sup>2</sup> M. Horio,<sup>2</sup> O. Ivashko,<sup>2</sup> N. E. Shaik,<sup>3</sup> K. von Arx,<sup>2</sup> Y. Sassa,<sup>6</sup> E. Paris,<sup>7</sup> M. H. Fischer,<sup>2</sup> Y. Tseng,<sup>7</sup> N. B. Christensen,<sup>8</sup> A. Galdi,<sup>9, 10</sup> D. G. Schlom,<sup>10, 11</sup> K. M. Shen,<sup>12</sup> T. Schmitt,<sup>7</sup> H. M. Rønnow,<sup>3</sup> and J. Chang<sup>2, †</sup>

<sup>1</sup>Department of Physics, The Chinese University of Hong Kong, Shatin, Hong Kong, China

<sup>2</sup>Physik-Institut, Universität Zürich, Winterthurerstrasse 190, CH-8057 Zürich, Switzerland

<sup>3</sup>Institute of Physics, École Polytechnique Fédérale de Lausanne (EPFL), CH-1015 Lausanne, Switzerland

<sup>4</sup>Institute of High Energy Physics, Chinese Academy of Sciences (CAS), Beijing 100049, China

<sup>5</sup>Spallation Neutron Source Science Center (SNSSC), Dongguan 523803, China

<sup>6</sup>Department of Physics, Chalmers University of Technology, SE-412 96 Göteborg, Sweden

<sup>7</sup>Swiss Light Source, Paul Scherrer Institut, CH-5232 Villigen PSI, Switzerland

<sup>8</sup>Department of Physics, Technical University of Denmark, DK-2800 Kongens Lyngby, Denmark

<sup>9</sup>Dipartimento di Ingegneria Industriale, Università degli Studi di Salerno, Fisciano (SA) 84084, Italy

<sup>10</sup>Department of Materials Science and Engineering,

Cornell University, Ithaca, New York 14850, USA

<sup>11</sup>Kavli Institute at Cornell for Nanoscale Science, Ithaca, New York 14853, USA

<sup>12</sup>Department of Physics, Laboratory of Atomic and Solid State Physics,

Cornell University, Ithaca, New York 14853, USA

**Quantum fluctuations in low-dimensional systems and near quantum phase transitions have significant influences on material properties. Yet, it is difficult to experimentally gauge the strength and importance of quantum fluctuations. Here we provide a resonant inelastic x-ray scattering study of magnon excitations in Mott insulating cuprates. From the thin film of  $\text{SrCuO}_2$ , single- and bi-magnon dispersions are derived. Using an effective Heisenberg Hamiltonian generated from the Hubbard model, we show that the single magnon dispersion is only described satisfactorily when including significant renormalization stemming from quantum fluctuations. Comparative results on  $\text{La}_2\text{CuO}_4$  indicate that quantum fluctuations are much stronger in  $\text{SrCuO}_2$  suggesting closer proximity to a magnetic quantum critical point. Monte Carlo calculations suggest an exotic incommensurate magnetic order as the ground state that competes with the antiferromagnetic Néel order. Our results indicate that  $\text{SrCuO}_2$ —due to strong quantum fluctuations—is a unique starting point for the exploration of novel magnetic ground states.**

One of the most studied electronic models is that of a two-dimensional square lattice [1]. At half-filling, when Coulomb interaction  $U$  overwhelms greatly the kinetic energy scale  $t$  the system crystallizes into an antiferromagnetically (AF) ordered Mott insulating state [2]. The physics of this system is well captured by the Hubbard model, from which an effective Heisenberg model can be generated to describe the AF ground state. In this

strong-coupling limit, the spin exchange interactions are realized through virtual hopping processes. Upon down-tuning the interaction strength, the AF Mott state remains a theoretical ground state. However, in this limit, small perturbations (for example doping) can trigger new magnetic or metallic ground states. Pushing the Mott state into this soft regime is therefore of great interest. When potential and kinetic energy scales are comparable, quantum fluctuations enter the problem. Many experimental and theoretical studies have addressed this intermediate region of  $U/t$ . Upon doping, high-temperature superconductivity has been found [3] and spin-liquid states are predicted in certain models [4]. On an experimental level, it has however been difficult to measure or gauge the strength of quantum fluctuations. Magnon excitations [5] of the Néel state should, in principle, be influenced by quantum fluctuations. The magnon dispersion is described by  $\hbar\omega = Z_c(k)\epsilon_k$ , where  $\epsilon_k$  is the “bare” magnon dispersion set by potential and kinetic energy scales, and  $Z_c(k) = Z_c^0(1 + f_k)$  is the renormalization factor stemming from quantum fluctuations with  $f_k$  being a momentum dependent function. In the strong coupling limit ( $U/t \rightarrow \infty$ ) quantum fluctuations are negligible implying  $f_k \rightarrow 0$  and  $Z_c(k) \approx 1.18$  is essentially momentum independent [6, 7]. As quantum fluctuations grow stronger with gradually moderate values of  $U/t$ , the renormalization factor  $Z_c(k)$  increases and acquires momentum dependence through a non-negligible  $f_k$ . This limit governed by quantum fluctuations is interesting as it may provide physics beyond the antiferromagnetic Néel state.

Conceptually, this moderate  $U/t$  limit is complicated due to a multitude of comparable magnetic exchange interactions. Nearest and next-nearest neighbour exchange interactions are given by  $J_1 = 4t^2/U$  and  $J_2 = 4t^4/U^3$ , in the projection of the Hubbard onto the Heisenberg model. In the moderate or weak interaction limit, higher-order exchange interaction terms are gaining prominence.

\* [qwang@cuhk.edu.hk](mailto:qwang@cuhk.edu.hk)

† [johan.chang@physik.uzh.ch](mailto:johan.chang@physik.uzh.ch)

The ring-exchange interaction  $J_{\square} = 80t^4/U^3$  becomes a significant fraction of  $J_1$  ( $J_{\square}/J_1 = 20t^2/U^2$ ) and manifests by a magnon zone-boundary dispersion [8–13]. In this limit, higher-order hopping integral  $t'$ , can introduce new magnetic interaction term  $J' = 4t'^2/U$  that further adds to enhance the zone boundary (ZB) dispersion. Within the Hubbard-Heisenberg model, the zone boundary dispersion, quantum fluctuations, and  $Z_c$  correlate in the  $U/t$  and  $t'/t$  parameter space. In fact, the renormalization factor  $Z_c$  gains its momentum dependence from the higher-order exchange interactions. Enhanced quantum fluctuations may thus introduce new magnetic ground states and with that exotic magnonic quasiparticles [14, 15]. It is thus interesting to study materials with significant higher-order exchange couplings. In the cuprates,  $ACuO_2$  with  $A = Sr, Ca$  has been studied with electron spectroscopy and resonant inelastic x-ray scattering (RIXS) [13, 14, 16] due to its large ring exchange interaction. Yet, no experiments have demonstrated the importance of quantum fluctuations through direct measurements of a momentum dependent magnon renormalization factor.

Here we provide a RIXS study of  $SrCuO_2$  (SCO) realized in thin film format. Analysis of the RIXS spectra led us to derive the single- and bi-magnon dispersions. Starting from an effective Heisenberg representation of the Hubbard model, we show that the observed single magnon dispersion is inconsistent with a constant  $Z_c$  for reasonable values of kinetic energy scales. We thus conclude that, in  $SrCuO_2$ , quantum fluctuations are significantly influencing the magnon dispersion. Further, our analysis shows that the observed magnon dispersion is well described when introducing significant momentum dependence to  $Z_c$ . Our results thus provide a gauge for quantum fluctuations which are getting increasingly important as  $U/t$  is down-tuned. Possible exotic magnetic ground states, emerging from quantum fluctuations are here explored by classical Monte Carlo calculations.

## Results

Crystal field environment around the copper site in  $SrCuO_2$  is shown schematically in Fig. 1a. In contrast to for example  $La_2CuO_4$  (LCO), no apical oxygen is present in  $SrCuO_2$ . Examples of Cu  $L$ -edge RIXS spectra, covering magnetic and  $dd$  excitations, are shown in Fig. 1b. The absence of the apical oxygen in  $SrCuO_2$  pushes the  $d_{z^2}$  excitation well below the  $t_{2g}$  excitations—as previously established in  $CaCuO_2$  [13, 18]. The two excitations at 1.43 and 1.73 eV are assigned to the  $d_{xy}$  and degenerated  $d_{xz}/d_{yz}$  states, respectively. The origin of the additional peak at  $\sim 2.06$  eV, which has also been observed in  $CaCuO_2$  [13, 18], is not fully understood.

Magnetic excitations have been recorded systematically along the antinodal  $(h, 0)$ , nodal  $(h, h)$  and zone boundary (azimuthal  $\phi$  rotation with a constant in-plane momentum amplitude  $Q_{\parallel\parallel}$ ) directions with both linear vertical ( $\sigma$ ) and linear horizontal ( $\pi$ ) incident light polar-

izations. A single magnon excitation manifests clearly in the  $\pi$  channel (see Fig. 1). When switching to  $\sigma$  polarization, the single magnon is suppressed (as expected [19]), and an excitation at higher energy appears. We interpret this as a magnetic continuum that in  $SrCuO_2$  (and  $CaCuO_2$ ) has a structure—sometimes referred to as a bi-magnon excitation [20–22]. In what follows, we extract the single magnon and bi-magnon dispersion along the high symmetry directions.

We analyze the low-energy part of the RIXS spectra by considering four components that include elastic scattering (enhanced in the  $\sigma$  channel [19]), single- and bi-magnon excitations, and a smoothly varying background. Elastic scattering is mimicked by a Gaussian function with the standard deviation set by the instrumental resolution and the peak centred at zero energy loss. The single- and bi-magnon excitations are described respectively by a damped harmonic oscillator convoluted with the instrumental resolution and a Gaussian function. Background is modeled by a second-order polynomial. In grazing-exit geometry, RIXS cross section from the magnon (bi-magnon) is generally enhanced when using the  $\pi$  ( $\sigma$ ) polarized incident lights—as shown in Fig. 1c,d. We fit globally across the two light polarizations to extract the two magnetic contributions. The resulting single- and bi-magnon dispersions are plotted on top of the inelastic RIXS spectral weight ( $\pi$  polarization) in Fig. 2a-c. Consistent with previous reports on  $CaCuO_2$  [13, 14], a large zone boundary dispersion  $E_{ZB} = \hbar\omega(\frac{1}{2}, 0) - \hbar\omega(\frac{1}{4}, \frac{1}{4})$  of the single magnon excitation is observed with an essentially non-dispersive section along the  $(h, h)$  direction. The bi-magnon dispersion  $\hbar\omega_{bm}$  roughly mimics the single magnon dispersion  $\hbar\omega_{sm}$ . At the zone boundary position  $(\frac{1}{4}, \frac{1}{4})$ ,  $\omega_{bm}/\omega_{sm} \approx 2$ . This ratio however varies significantly along the high symmetry directions.

The fitting of the single- and bi-magnon excitations also provides information about spectral weight and quasiparticle lifetime. For most of the Brillouin zone, the energy width of the single magnon is resolution-limited. However, around  $(0.5, 0)$  spectral weight suppression and shorter single magnon lifetimes are observed consistently with what has previously been reported in  $La_2CuO_4$  and  $CaCuO_2$  [10, 13, 14].

## Discussion

The single magnon dispersion of  $SrCuO_2$  features two peculiar characteristics. A steep zone boundary dispersion is followed by a non-dispersive section along the  $(h, h)$  direction. Magnon excitations of layered copper-oxides have been discussed via a Heisenberg Hamiltonian derived from the Hubbard model [2]. In the simplest form, the nearest-neighbour exchange interaction  $J_1 = 4t^2/U$  is described through the Coulomb interaction  $U$  and nearest-neighbour hopping integral  $t$ . The magnon dispersion is, in this limit, isotropic—given by  $\hbar\omega = 2J_1(1 - ((\cos(Q_x) + \cos(Q_y))/2)^2)^{1/2}$ . Early neutron scattering experiments on  $La_2CuO_4$  [8], however, revealed a

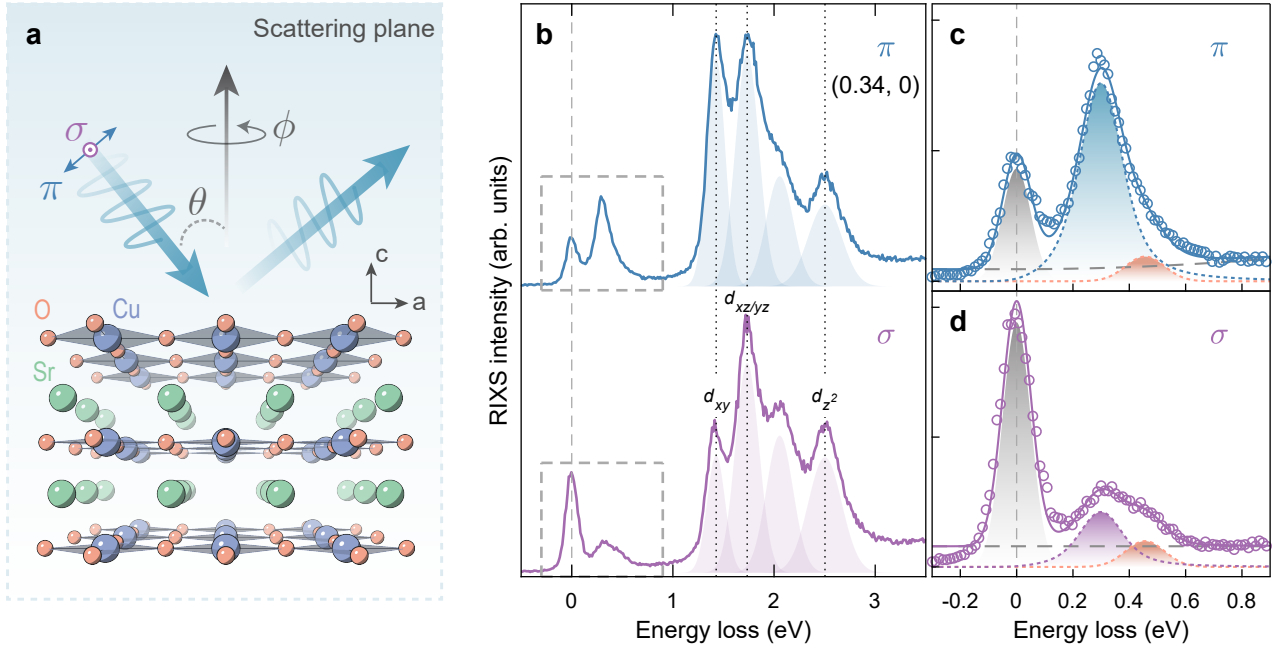


FIG. 1. **RIXS on SrCuO<sub>2</sub> with different incident light polarizations.** (a) Crystal structure of SrCuO<sub>2</sub> and schematic illustration of the RIXS scattering geometry. Incident light, either linear horizontal ( $\pi$ ) or vertical ( $\sigma$ ), is directed to the film with variable angle  $\theta$ . (b) RIXS spectra at  $\mathbf{Q} = (0.34, 0)$  measured with  $\pi$  (blue line) and  $\sigma$  (purple line) incident x-rays. Spectra are vertically shifted for clarity. Dotted lines mark the peak positions of the  $dd$  excitations, determined from fitting with Gaussian components denoted by the shaded areas. (c,d) Zooms of the low-energy part (within the grey dashed boxes) of the spectra in (b). Solid lines are the sum of a four-component fit. Each component is indicated by dashed lines and shaded areas—see text for detailed information. Vertical dashed lines indicate the zero energy loss.

zone boundary dispersion indicating the importance of higher-order exchange interaction terms. To account for this zone boundary term, a circular magnetic exchange interaction  $J_{\square} \sim t^4/U^3$  was included to satisfactorily describe the observed magnon dispersion [8, 10]. Later more detailed studies [17, 23] included higher-order hopping terms, i.e., next, and next-next nearest-neighbour hopping intergrals  $t'$  and  $t''$ . This extended model, yields a magnon dispersion  $\hbar\omega = Z_c(U, t, t', t'')\epsilon_k(U, t, t', t'')$ , where  $Z_c$  is a momentum dependent quantum renormalization factor and  $\epsilon_k(U, t, t', t'') = \sqrt{A_k^2 - B_k^2}$  is the bare magnon dispersion with  $A_k$  and  $B_k$  determined by  $U$ ,  $t$ ,  $t'$ , and  $t''$ , as described in Refs. 17 and 23. In the  $U/t \rightarrow \infty$  limit, the magnon-magnon renormalization factor  $Z_c$  is momentum independent, and  $\epsilon_k(U, t, t', t'')$  has an analytic expression [12, 24]. This expression has been used to fit the magnon dispersion of La<sub>2</sub>CuO<sub>4</sub>, with realistic values of  $U, t$ ,  $t'$  and  $t''$ . In particular, ratios of  $t'/t \sim -0.4$  and  $t''/t \sim 0.2$  are found consistent with ARPES experiments [12, 25].

For SrCuO<sub>2</sub>, however, the constant  $Z_c$  solution does not provide a satisfactory description of the observed single magnon dispersion (see blue dashed lines in Fig. 3g-1). As La<sub>2</sub>CuO<sub>4</sub> and SrCuO<sub>2</sub> share similar square lattice structures, similar values of  $t'/t$  are expected. However, an unbiased fit yields unphysical values ( $t'/t > 0$ ) for the hopping parameters and physical sensible values provide

poor fits. We are thus led to reject the initial ansatz  $Z_c = Z_c^0(1 + f_k) \approx Z_c^0$  with  $f_k \rightarrow 0$  and hence  $Z_c$  being a momentum independent constant.

Consequently, we fit  $\hbar\omega = Z_c(U, t, t', t'')\epsilon_k(U, t, t', t'')$  in a numerical self-consistent fashion. For La<sub>2</sub>CuO<sub>4</sub>, this methodology confirms that  $Z_c$  is roughly constant (see Fig. 3a-c and Table I) with marginal changes to  $U, t, t', t''$  (compared to the constant  $Z_c$  model [12]). However, for SrCuO<sub>2</sub>, an entirely new solution emerges. Values of  $t'/t$  and  $t''/t$  comparable to La<sub>2</sub>CuO<sub>4</sub> and a smaller  $U/t$  now describes the magnon dispersion—see solid lines in Fig. 3 and Table I. We stress that this new solution describes the observed dispersion using fewer fitting parameters as  $Z_c$  is now given by  $U, t, t', t''$ . The moderate value of  $U/t$  implies a magnon-magnon renormalization factor that is strongly momentum dependent (see Fig. 3g-i), i.e.,  $f_k$  in  $Z_c = Z_c^0(1 + f_k)$  is no longer negligible. Our results thus indicate that quantum fluctuations have a significant impact on the magnon dispersion in SrCuO<sub>2</sub>.

In Fig. 4, we plot the constant  $\chi^2$  (goodness-of-fit) contour lines that encircle solutions that are within 10% of the minimum of  $\chi^2$ . With the currently available data, a rather broad set of parameters describe the magnon dispersion of La<sub>2</sub>CuO<sub>4</sub>. For SrCuO<sub>2</sub>, however,  $\chi^2$  has a unique well-defined minimum confined to a narrow region of the parameter space. In Table I, the fitting values to describe the magnon dispersions for La<sub>2</sub>CuO<sub>4</sub> and

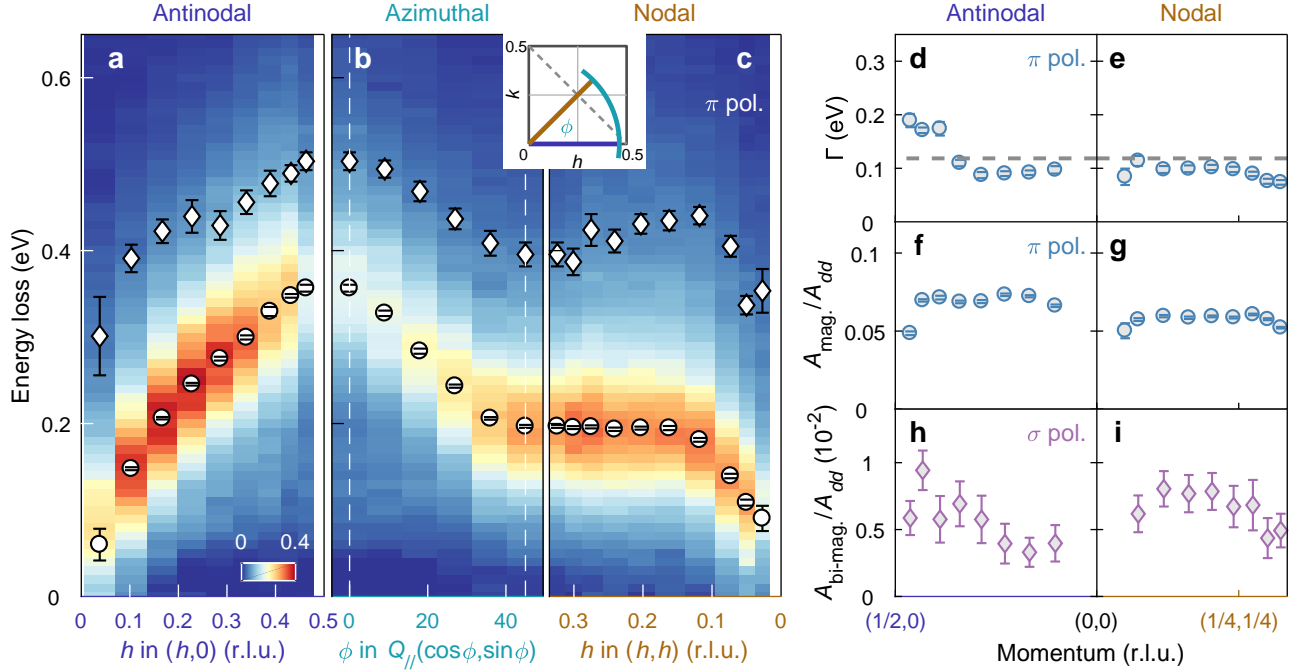


FIG. 2. **Magnon and bi-magnon dispersion and spectral weight observed in  $\text{SrCuO}_2$ .** (a-c) RIXS intensity as a function of momentum and energy loss measured with  $\pi$  polarized incident light, along three different directions in the reciprocal space as indicated by the solid color lines in the inset. Elastic and background scattering has been subtracted. Open circles and diamond points indicate respectively the magnon and bi-magnon pole position (see text for detailed description of the analysis). In (b) the in-plane momentum amplitude is  $Q_{\parallel} = 0.463$ . (d,e) Single magnon inverse lifetime  $\Gamma \sim \hbar/\tau$  along the anti-nodal and nodal directions. Horizontal dashed line indicates the applied energy resolution. (f-i) Normalized single-magnon (f,g) and bi-magnon (h,i) spectral weight along the  $(h, 0)$  and  $(h, h)$  high symmetry directions. Error bars are determined from the fitting uncertainty.

$\text{SrCuO}_2$  are listed. For  $\text{SrCuO}_2$ , these values represent a minimum in the  $\chi^2$  function. For  $\text{La}_2\text{CuO}_4$ , we further constrain the solutions by fixing  $t'/t = -0.4$ . In Fig. 4, the modeled zone boundary dispersion is plotted as a function of  $J_{\square}/J_1$  and  $J'/J_1$ . Within the same parameter space, the Brillouin zone average  $\bar{Z}_c$  is shown. Generally, the model displays a correlation between magnon ZB dispersion and  $\bar{Z}_c$ . The Heisenberg-Hamiltonian projection from Hubbard model is breaking down in the limit where  $\bar{Z}_c \gg Z_c^0$ —that is when  $(J_{\square} + J')/J_1$  is large.

Compared to  $\text{La}_2\text{CuO}_4$ ,  $\text{SrCuO}_2$  displays a larger ring exchange coupling  $J_{\square}$ . In fact, the fitting parameters obtained for  $\text{SrCuO}_2$  are close to the limit where the Heisenberg representation of the Hubbard model breaks down. This limit is characterized by a complete suppression of the staggered magnetization and the imaginary solution of the magnon dispersion (Fig. 4). We thus demonstrate that  $\text{SrCuO}_2$  hosts strong quantum fluctuations that can potentially stabilize ground states beyond the AF ordered Néel state. Enhancing further  $J_{\square}/J_1$  or  $J'/J_1$  would be of great interest to explore new quantum matter ground states.

To gain insight into the possible magnetic ground

states when the Néel order breaks down by the increase of  $t$  and  $t'$ , we perform Monte Carlo calculations using a Heisenberg Hamiltonian including the first-, second-, and third-nearest-neighbour, as well as a four-spin ring exchange coupling (see Methods). To compare with the experimental results on  $\text{SrCuO}_2$ , we fixed  $U = 2.66$  eV and  $t''/t' = -0.5$ . Incommensurate magnetic orders characterized by a quartet of magnetic Bragg peaks around  $(0.5, 0.5)$ , i.e., with wave vectors  $\mathbf{Q}_M = (0.5 \pm \delta, 0.5)$  and  $(0.5, 0.5 \pm \delta)$ , or  $\mathbf{Q}_M = (0.5 \pm \delta/\sqrt{2}, 0.5 \pm \delta/\sqrt{2})$  are found in the parameter space between the antiferromagnetic Néel and columnar orders (see Supplementary Fig. 1 for examples of the calculated spin structure factor). We plot in Fig. 4d the distance  $\delta$  between  $\mathbf{Q}_M$  and the Néel wave vector  $(0.5, 0.5)$  as a function of  $t$  and  $t'/t$ . While  $\text{SrCuO}_2$  is in the Néel AF ordered state, it is located not far from incommensurate magnetic ordered phases which can be reached by increasing  $t$ . Further increase of  $t'/t$  enhances the next-nearest neighbour coupling and stabilizes the columnar antiferromagnetic order. This tuning can be potentially realized by strain application with different substrates [12, 26]. We point

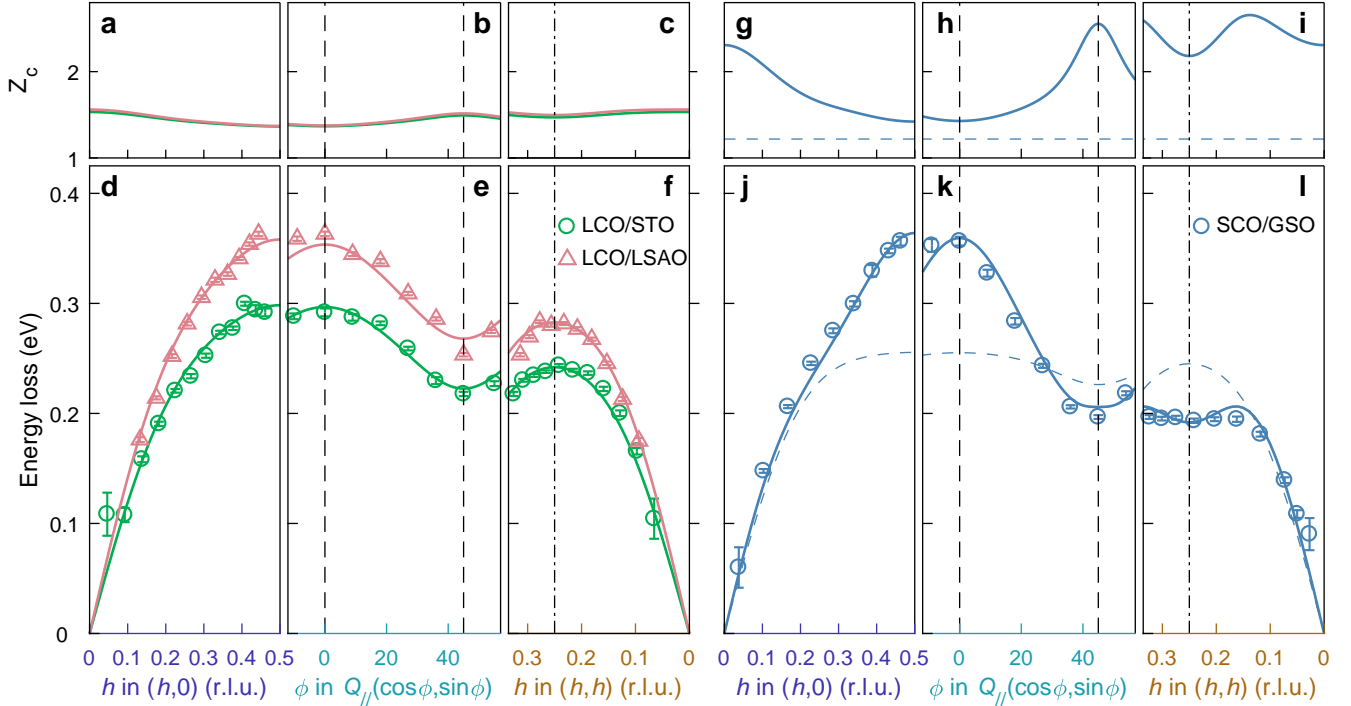


FIG. 3. **Magnon dispersion and momentum dependence of quantum fluctuation factor  $Z_c$ .** Bottom panels display the magnon dispersion along the indicated momentum trajectories for LCO/STO (green), LCO/LSAO (pink), and SCO/GSO (blue). Corresponding solid lines are fits using a Hubbard model (see text) including higher-order terms. Fitting values are listed in Table I. Top panels display the momentum dependence of the quantum fluctuation factor  $Z_c$  obtained from fitting with the Hubbard model. Blue dashed lines mark the magnon dispersion obtained assuming a constant  $Z_c = 1.219$  [12, 17], with  $U = 2.18$ ,  $U/t = 6.25$ ,  $t'/t = -0.4$ , and  $t''/t' = -0.5$ . Error bars indicate one standard deviation. The in-plane momentum amplitude  $Q_{//}$  takes 0.461, 0.444, and 0.463 for LCO/STO, LCO/LSAO, and SCO/GSO, respectively. Data on LCO/STO and LCO/LSAO are taken from ref. [12].

out that the classical Monte Carlo simulations do not capture the quantum nature of the problem, but they show the parameter space where the Néel state is expected to break down. When the magnetic order is suppressed by the strong quantum fluctuations near the phase boundary, superconductivity could be potentially enhanced. It would therefore be of great interest to study how the different magnetic ground states influence superconductivity upon doping.

## Methods

**Film growth.** High-quality  $\text{SrCuO}_2$  and  $\text{La}_2\text{CuO}_4$  thin films were grown using Molecular Beam Epitaxy (MBE). The  $\text{SrCuO}_2$  ( $\sim 15$  nm) film is deposited on a (110)  $\text{GdScO}_3$  (GSO) substrate [29, 30], and  $\text{La}_2\text{CuO}_4$  films are grown on (001)  $\text{SrTiO}_3$  (STO) and  $\text{LaSrAlO}_4$  (LSAO) substrates, with a thickness of 7-8 and 18-19 nm, respectively [12].

**RIXS experiments.** Cu  $L_3$ -edge RIXS experiments were carried out at the ADRESS beamline [31, 32], of the

Swiss Light Source (SLS) synchrotron at the Paul Scherrer Institut. All data were collected at base temperature ( $\sim 20$  K) under ultrahigh vacuum (UHV) conditions,  $10^{-9}$  mbar or better. RIXS spectra were acquired in grazing-exit geometry with both linear horizontal ( $\pi$ ) and linear vertical ( $\sigma$ ) incident light polarisations with a fixed scattering angle  $2\theta = 130^\circ$ . The energy resolution, estimated by the half-width-at-half-maximum of the elastic scattering from an amorphous carbon sample, is 68 meV at Cu  $L_3$  edge ( $\sim 931.5$  eV). Momentum transfer is expressed in reciprocal lattice units (r.l.u.) using a pseudo-tetragonal unit cell with  $a = b = 3.97$  Å and  $c = 3.4$  Å for  $\text{SrCuO}_2$ ,  $a = b = 3.8$  Å and  $c = 13.2$  Å for  $\text{La}_2\text{CuO}_4$ . RIXS intensities are normalised to the weight of  $dd$  excitations [33].

**Modelling of magnon.** Fitting of the magnon dispersion was done by calculating self-consistently  $Z_c$  and  $\epsilon_k$  in  $\hbar\omega = Z_c(U, t, t', t'')\epsilon_k(U, t, t', t'')$ . We used  $t''/t' = -0.5$  [27]. Fitting parameters  $U$  and  $t$  were ob-

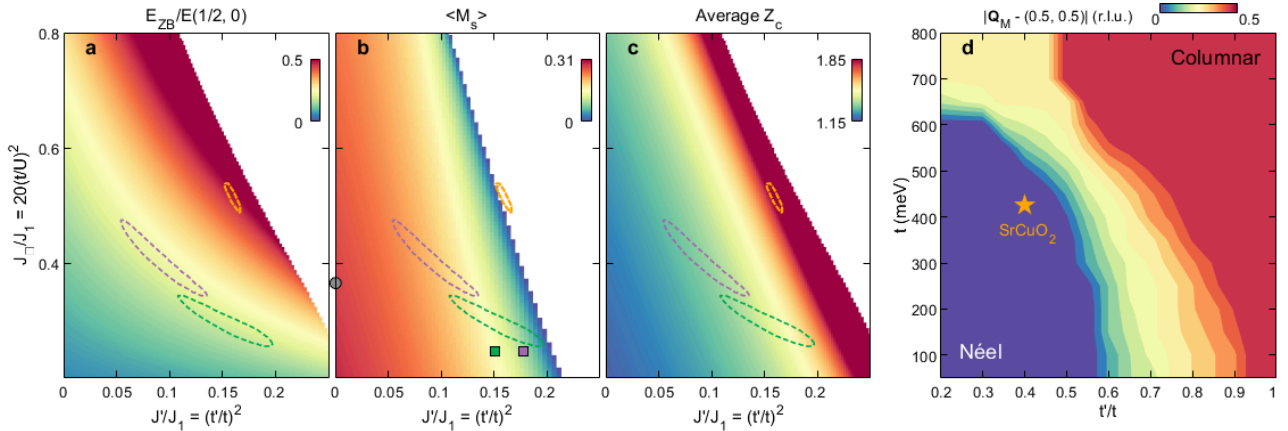


FIG. 4. **Quantum fluctuation renormalization factor within the Hubbard model.** (a,b) Zone boundary dispersion ratio  $E_{ZB}/E(1/2, 0)$ , renormalized staggered magnetization as a function of the exchange interactions  $J_□/J_1$  and  $J'/J_1$ . (c) Average renormalization factor  $Z_c$  across the Brillouin zone for the same parameter space as in (a,b). Green, pink, and orange dashed circles indicate constant  $\chi^2$  contour lines with solutions that are within 10% of the minimum of  $\chi^2$  for LCO/STO, LCO/LSAO, and SCO, respectively. Grey, green, and purple filled symbols denote parameters determined from the Hubbard model with constant  $Z_c$  on respectively bulk LCO [8], LCO/STO, and LCO/LSAO [12]. Empty areas in (a,c) and (b) indicate where the magnon dispersion becomes imaginary and the negative magnetization, respectively. (d) Magnetic ground state structure as a function of  $t$  and  $t'/t$  obtained from Monte Carlo calculations with  $U = 2.66$  eV and  $t''/t' = -0.5$  fixed. Orange pentagram marks the position of SCO.

TABLE I. **Hubbard model parameters for magnons in  $\text{La}_2\text{CuO}_4$  and  $\text{SrCuO}_2$  films.** Nearest, next-nearest neighbour hopping integral  $t$ ,  $t'$ , and Coulomb interaction  $U$  are obtained through self-consistent fitting the observed single magnon dispersion. Ratio between the next-nearest hopping integral  $t''$  and  $t'$  was fixed to literature values [25, 27, 28]. Resulting electron correlation strength  $U/t$  is anti-correlated with the zone boundary dispersion ratio  $E_{ZB}/E(1/2, 0)$ , average ( $\bar{Z}_c$ ), and variation ( $\Delta Z_c$ ) of  $Z_c$  across the Brillouin zone.

Sample	$t$ [meV]	$U$ [eV]	$-t'/t$	$-t''/t'$	$U/t$	$\bar{Z}_c$	$\Delta Z_c/\bar{Z}_c[\%]$	$E_{ZB}/E(1/2, 0)[\%]$
LCO/STO	408	3.38	0.4	0.5	8.33	1.45	11.6	18.9
LCO/LSAO	474.9	3.83	0.4	0.5	8.06	1.47	12.9	21.1
SCO/NGO	425.6	2.66	0.4	0.5	6.25	1.91	64.5	47.3

tained by minimizing  $\chi^2$ . The staggered magnetization is calculated by  $\langle M_s^\dagger \rangle = (S + \frac{1}{2} - \frac{2}{N} \sum_{\mathbf{k}} \frac{A_{\mathbf{k}}}{2\epsilon_{\mathbf{k}}})(1 - 8t^2/U^2)$ , where  $N$  is the number of spin on the square lattice. Our code is available upon request.

**Monte Carlo simulations.** Monte Carlo simulations were carried out using the Heisenberg Hamiltonian projected from the Hubbard model, taking into consideration the leading contributions of  $t'$  and  $t''$ :

$$\begin{aligned} \hat{\mathcal{H}} = & J \sum_{\langle i,j \rangle} \mathbf{S}_i \cdot \mathbf{S}_j + (J_2 + J') \sum_{\langle i,i' \rangle} \mathbf{S}_i \cdot \mathbf{S}_{i'} \\ & + (J_3 + J'') \sum_{\langle i,i'' \rangle} \mathbf{S}_i \cdot \mathbf{S}_{i''} + J_□ \sum_{\langle i,j,k,l \rangle} [(\mathbf{S}_i \cdot \mathbf{S}_j)(\mathbf{S}_k \cdot \mathbf{S}_l) \\ & + (\mathbf{S}_i \cdot \mathbf{S}_l)(\mathbf{S}_k \cdot \mathbf{S}_j) - (\mathbf{S}_i \cdot \mathbf{S}_k)(\mathbf{S}_j \cdot \mathbf{S}_l)], \end{aligned}$$

where  $J = J_1 - \frac{24t^4}{U^3}$ ,  $J_1 = \frac{4t^2}{U}$ ,  $J_2 = \frac{J_3}{J_1} = \left(\frac{t}{U}\right)^2$ ,  $J' = \left(\frac{t'}{t}\right)^2$ ,  $J'' = \left(\frac{t''}{t}\right)^2$  and  $J_□ = 20\left(\frac{t}{U}\right)^2$ . The first three sums count respectively nearest, next-nearest, and

next-next-nearest neighbour using indices  $\langle i,j \rangle$ ,  $\langle i,i' \rangle$  and  $\langle i,i'' \rangle$ . The last sum counts around the squares following the clockwise direction. Simulations were performed at 0.1 K on a sheet of  $50 \times 50$  unit cells in the  $(a,b)$ -plane, i.e., 2500 magnetic sites with classical spin  $S = \frac{1}{2}$ . For each set of input values,  $(U, t, t', t'')$ , the simulation ran for  $10^7$  Monte Carlo Steps with random starting configurations. The Monte Carlo calculation code is available upon request.

**Acknowledgments** We thank André-Marie Tremblay, Michel Gingras, Takami Tohyama, and Krzysztof Wohlfeld for insightful discussions. RIXS measurements were performed at the ADRESS beamline of the SLS at the Paul Scherrer Institut, Villigen PSI, Switzerland. We thank the ADRESS beamline staff for technical support. M.H., O.I., K.v.A., N.A., E.P., Y.T., T.S. and J.C. acknowledge support by the Swiss National Science Foundation through grant numbers PP00P2\_176877, 200021\_188564, CRSII2\_160765/1 and BSSGI0\_155873.

Q.W. is supported by the Research Grants Council of Hong Kong (ECS No. 24306223), and the CUHK Direct Grant (No. 4053613). Work at Cornell was supported by the Air Force Office of Scientific Research grant number FA9550-21-1-0168 and the National Science Foundation through NSF DMR-2104427. I.B. acknowledges sup-

port from the Federal Commission for Scholarships for Foreign Students for the Swiss Government Excellence (ESKAS No. 2022.0001) for the academic year 2022-23. E.F. and H.M.R. acknowledge support by the European Research Council through the Synergy network HERO (Grant No. 810451).

---

[1] H.-C. Jiang and T. P. Devereaux, Superconductivity in the doped hubbard model and its interplay with next-nearest hopping  $t'$ , *Science* **365**, 1424 (2019).

[2] M. Imada, A. Fujimori, and Y. Tokura, Metal-insulator transitions, *Rev. Mod. Phys.* **70**, 1039 (1998).

[3] P. A. Lee, N. Nagaosa, and X.-G. Wen, Doping a Mott insulator: Physics of high-temperature superconductivity, *Rev. Mod. Phys.* **78**, 17 (2006).

[4] Y. Zhou, K. Kanoda, and T.-K. Ng, Quantum spin liquid states, *Rev. Mod. Phys.* **89**, 025003 (2017).

[5] L. Braicovich, J. van den Brink, V. Bisogni, M. M. Sala, L. J. P. Ament, N. B. Brookes, G. M. De Luca, M. Saluzzo, T. Schmitt, V. N. Strocov, and G. Ghiringhelli, Magnetic excitations and phase separation in the under-doped  $\text{La}_{2-x}\text{Sr}_x\text{CuO}_4$  superconductor measured by resonant inelastic x-ray scattering, *Phys. Rev. Lett.* **104**, 077002 (2010).

[6] R. R. P. Singh, Thermodynamic parameters of the  $T=0$ , spin-1/2 square-lattice Heisenberg antiferromagnet, *Phys. Rev. B* **39**, 9760 (1989).

[7] C. M. Canali, S. M. Girvin, and M. Wallin, Spin-wave velocity renormalization in the two-dimensional Heisenberg antiferromagnet at zero temperature, *Phys. Rev. B* **45**, 10131 (1992).

[8] R. Coldea, S. M. Hayden, G. Aeppli, T. G. Perring, C. D. Frost, T. E. Mason, S.-W. Cheong, and Z. Fisk, Spin waves and electronic interactions in  $\text{La}_2\text{CuO}_4$ , *Phys. Rev. Lett.* **86**, 5377 (2001).

[9] A. A. Katanin and A. P. Kampf, Theoretical analysis of magnetic Raman scattering in  $\text{La}_2\text{CuO}_4$  : Two-magnon intensity with the inclusion of ring exchange, *Phys. Rev. B* **67**, 100404 (2003).

[10] N. S. Headings, S. M. Hayden, R. Coldea, and T. G. Perring, Anomalous high-energy spin excitations in the high- $T_c$  superconductor-parent antiferromagnet  $\text{La}_2\text{CuO}_4$ , *Phys. Rev. Lett.* **105**, 247001 (2010).

[11] N. B. Christensen, H. M. Rønnow, D. F. McMorrow, A. Harrison, T. G. Perring, M. Enderle, R. Coldea, L. P. Regnault, and G. Aeppli, Quantum dynamics and entanglement of spins on a square lattice, *Proc. Natl. Acad. Sci. U.S.A.* **104**, 15264 (2007).

[12] O. Ivashko, M. Horio, W. Wan, N. B. Christensen, D. E. McNally, E. Paris, Y. Tseng, N. E. Shaik, H. M. Rønnow, H. I. Wei, C. Adamo, C. Lichtensteiger, M. Gibert, M. R. Beasley, K. M. Shen, J. M. Tomczak, T. Schmitt, and J. Chang, Strain-engineering Mott-insulating  $\text{La}_2\text{CuO}_4$ , *Nat. Commun.* **10**, 786 (2019).

[13] Y. Y. Peng, G. Dellea, M. Minola, M. Conni, A. Amorese, D. Di Castro, G. M. De Luca, K. Kummer, M. Saluzzo, X. Sun, X. J. Zhou, G. Balestrino, M. Le Tacon, B. Keimer, L. Braicovich, N. B. Brookes, and G. Ghiringhelli, Influence of apical oxygen on the extent of in-plane exchange interaction in cuprate superconductors, *Nat. Phys.* **13**, 1201 (2017).

[14] L. Martinelli, D. Betto, K. Kummer, R. Arpaia, L. Braicovich, D. Di Castro, N. B. Brookes, M. Moretti Sala, and G. Ghiringhelli, Fractional spin excitations in the infinite-layer cuprate  $\text{CaCuO}_2$ , *Phys. Rev. X* **12**, 021041 (2022).

[15] B. D. Piazza, M. Mourigal, N. B. Christensen, G. J. Nilsen, P. Tregenna-Piggott, T. G. Perring, M. Enderle, D. F. McMorrow, D. A. Ivanov, and H. M. Rønnow, Fractional excitations in the square-lattice quantum antiferromagnet, *Nat. Phys.* **11**, 62 (2014).

[16] M. Dantz, J. Pelliciari, D. Samal, V. Bisogni, Y. Huang, P. Olalde-Velasco, V. N. Strocov, G. Koster, and T. Schmitt, Quenched magnon excitations by oxygen sublattice reconstruction in  $(\text{SrCuO}_2)_n/(\text{SrTiO}_3)_2$  superlattices, *Sci. Rep.* **6**, 32896 (2016).

[17] J.-Y. P. Delannoy, M. J. P. Gingras, P. C. W. Holdsworth, and A.-M. S. Tremblay, Low-energy theory of the  $t - t' - t'' - U$  Hubbard model at half-filling: Interaction strengths in cuprate superconductors and an effective spin-only description of  $\text{La}_2\text{CuO}_4$ , *Phys. Rev. B* **79**, 235130 (2009).

[18] M. Moretti Sala, V. Bisogni, C. Aruta, G. Balestrino, H. Berger, N. B. Brookes, G. M. d. Luca, D. Di Castro, M. Grioni, M. Guarise, P. G. Medaglia, F. Miletto Granizio, M. Minola, P. Perna, M. Radovic, M. Salluzzo, T. Schmitt, K. J. Zhou, L. Braicovich, and G. Ghiringhelli, Energy and symmetry of dd excitations in undoped layered cuprates measured by Cu  $L_3$  resonant inelastic x-ray scattering, *New J. Phys.* **13**, 043026 (2011).

[19] L. J. P. Ament, M. van Veenendaal, T. P. Devereaux, J. P. Hill, and J. van den Brink, Resonant inelastic x-ray scattering studies of elementary excitations, *Rev. Mod. Phys.* **83**, 705 (2011).

[20] L. Braicovich, L. J. P. Ament, V. Bisogni, F. Forte, C. Aruta, G. Balestrino, N. B. Brookes, G. M. De Luca, P. G. Medaglia, F. M. Granizio, M. Radovic, M. Saluzzo, J. van den Brink, and G. Ghiringhelli, Dispersion of magnetic excitations in the cuprate  $\text{La}_2\text{CuO}_4$  and  $\text{CaCuO}_2$  compounds measured using resonant x-ray scattering, *Phys. Rev. Lett.* **102**, 167401 (2009).

[21] V. Bisogni, L. Simonelli, L. J. P. Ament, F. Forte, M. Moretti Sala, M. Minola, S. Huotari, J. van den Brink, G. Ghiringhelli, N. B. Brookes, and L. Braicovich, Bi-magnon studies in cuprates with resonant inelastic x-ray scattering at the O  $K$  edge. I. Assessment on  $\text{La}_2\text{CuO}_4$  and comparison with the excitation at Cu  $L_3$  and Cu  $K$  edges, *Phys. Rev. B* **85**, 214527 (2012).

[22] L. Chaix, E. W. Huang, S. Gerber, X. Lu, C. Jia, Y. Huang, D. E. McNally, Y. Wang, F. H. Vernay, A. Keren, M. Shi, B. Moritz, Z.-X. Shen, T. Schmitt, T. P. Devereaux, and W.-S. Lee, Resonant inelastic x-ray scattering studies of magnons and bimagnons in the

lightly doped cuprate  $\text{La}_{2-x}\text{Sr}_x\text{CuO}_4$ , *Phys. Rev. B* **97**, 155144 (2018).

[23] B. Dalla Piazza, M. Mourigal, M. Guarise, H. Berger, T. Schmitt, K. J. Zhou, M. Grioni, and H. M. Rønnow, Unified one-band Hubbard model for magnetic and electronic spectra of the parent compounds of cuprate superconductors, *Phys. Rev. B* **85**, 100508 (2012).

[24] O. Ivashko, N. E. Shaik, X. Lu, C. G. Fatuzzo, M. Dantz, P. G. Freeman, D. E. McNally, D. Destraz, N. B. Christensen, T. Kurosawa, N. Momono, M. Oda, C. E. Matt, C. Monney, H. M. Rønnow, T. Schmitt, and J. Chang, Damped spin excitations in a doped cuprate superconductor with orbital hybridization, *Phys. Rev. B* **95**, 214508 (2017).

[25] C. E. Matt, D. Sutter, A. M. Cook, Y. Sassa, M. Måansson, O. Tjernberg, L. Das, M. Horio, D. Destraz, C. G. Fatuzzo, K. Hauser, M. Shi, M. Kobayashi, V. N. Strocov, T. Schmitt, P. Dudin, M. Hoesch, S. Pyon, T. Takayama, H. Takagi, O. J. Lipscombe, S. M. Hayden, T. Kurosawa, N. Momono, M. Oda, T. Neupert, and J. Chang, Direct observation of orbital hybridisation in a cuprate superconductor, *Nat. Commun.* **9**, 972 (2018).

[26] I. Biało, L. Martinelli, G. De Luca, P. Worm, A. Drewanowski, J. Choi, M. Garcia-Fernandez, S. Agrestini, K.-J. Zhou, L. Guo, C. B. Eom, J. M. Tomczak, K. Held, M. Gibert, Q. Wang, and J. Chang, Strain-tuned magnetic frustration in a square lattice  $J_1$ - $J_2$  material, [arXiv:2306.05828](https://arxiv.org/abs/2306.05828).

[27] T. Yoshida, X. J. Zhou, K. Tanaka, W. L. Yang, Z. Hussain, Z.-X. Shen, A. Fujimori, S. Sahrakorpi, M. Lindroos, R. S. Markiewicz, A. Bansil, S. Komiya, Y. Ando, H. Eisaki, T. Kakeshita, and S. Uchida, Systematic doping evolution of the underlying Fermi surface of  $\text{La}_{2-x}\text{Sr}_x\text{CuO}_4$ , *Phys. Rev. B* **74**, 224510 (2006).

[28] Y. Zhong, Z. Chen, S.-D. Chen, K.-J. Xu, M. Hashimoto, Y. He, S. ichi Uchida, D. Lu, S.-K. Mo, and Z.-X. Shen, Differentiated roles of Lifshitz transition on thermodynamics and superconductivity in  $\text{La}_2\text{CuO}_4$ , *Proc. Natl. Acad. Sci. U.S.A.* **119**, e2204630119 (2022).

[29] L. Maritato, A. Galdi, P. Orgiani, J. W. Harter, J. Schubert, K. M. Shen, and D. G. Schlom, Layer-by-layer shuttered molecular-beam epitaxial growth of superconducting  $\text{Sr}_{1-x}\text{La}_x\text{CuO}_2$  thin films, *J. Appl. Phys.* **113**, 053911 (2013).

[30] J. W. Harter, L. Maritato, D. E. Shai, E. J. Monkman, Y. Nie, D. G. Schlom, and K. M. Shen, Doping evolution and polar surface reconstruction of the infinite-layer cuprate  $\text{Sr}_{1-x}\text{La}_x\text{CuO}_2$ , *Phys. Rev. B* **92**, 035149 (2015).

[31] V. N. Strocov, T. Schmitt, U. Flechsig, T. Schmidt, A. Imhof, Q. Chen, J. Raabe, R. Betemps, D. Zimoch, J. Krempasky, X. Wang, M. P. A. Grioni, and L. Patthey, High-resolution soft X-ray beamline ADDRESS at the Swiss Light Source for resonant inelastic X-ray scattering and angle-resolved photoelectron spectroscopies, *J. Synchrotron Radiat.* **17**, 631 (2010).

[32] G. Ghiringhelli, A. Piazzalunga, C. Dallera, G. Trezzi, L. Braicovich, T. Schmitt, V. N. Strocov, R. Betemps, L. Patthey, X. Wang, and M. Grioni, SAXES, a high resolution spectrometer for resonant x-ray emission in the 400-1600 eV energy range, *Rev. Sci. Instrum.* **77**, 113108 (2006).

[33] Q. Wang, M. Horio, K. von Arx, Y. Shen, D. John Mukkattukavil, Y. Sassa, O. Ivashko, C. E. Matt, S. Pyon, T. Takayama, H. Takagi, T. Kurosawa, N. Momono, M. Oda, T. Adachi, S. M. Haidar, Y. Koike, Y. Tseng, W. Zhang, J. Zhao, K. Kummer, M. Garcia-Fernandez, K.-J. Zhou, N. B. Christensen, H. M. Rønnow, T. Schmitt, and J. Chang, High-temperature charge-stripe correlations in  $\text{La}_{1.675}\text{Eu}_{0.2}\text{Sr}_{0.125}\text{CuO}_4$ , *Phys. Rev. Lett.* **124**, 187002 (2020).